# Behavior of Absorbed Water in Elongated Polyamide 6

**Eiichi Sakai, Makoto Kawagoe**

*Department of Mechanical Systems Engineering, Faculty of Engineering, Toyama Prefectural University, 5180 Kurokawa, Imizu, Toyama 939–0398, Japan*

Received 17 April 2009; accepted 13 August 2009
DOI 10.1002/app.31274
Published online 15 September 2009 in Wiley InterScience (www.interscience.wiley.com).

**ABSTRACT:** The state of absorbed water in polyamide 6 elongated to several levels have been investigated in relation to the polymer microstructure. The absorption behavior of distilled water at 20°C was monitored until the saturation. Both the diffusion coefficient and the equilibrium content of water were increased by plastic elongation. The large elongation caused a reduction in the storage modulus and rises in the loss tangents for α- and β-relaxations. The DSC measurements clearly indicated several exothermic peaks showing the presence of freezable bound water in the largely elongated specimen. These results suggest that some microstructural defects like voids are formed by the collapse of crystals by large elongation, and the water molecules are accumulated in such defects under weaker interaction with the surrounding polymer. Supposing the pore as the structural defect, the pore size distribution was obtained from the DSC curve by the method of thermoporosimetry. Assuming the cylindrical pores, they were characterized to have the total volume of about $13.5 \times 10^{-4}$ mm$^3$ g$^{-1}$, the surface area of about 1.1 m$^2$ g$^{-1}$, and the average radius of about 2.5 nm, being appropriately called mesopore. © 2009 Wiley Periodicals, Inc. J Appl Polym Sci 115: 1272–1277, 2010

**Key words:** polyamides; diffusion; freezable bound water; differential scanning calorimetry (DSC); thermoporosimetry

## INTRODUCTION

Since the water in solid polymers generally exerts considerable influences on their mechanical properties, the evaluation of absorption behavior and the existing state of water in solid polymers are of great significance, and thus have been extensively studied.[1–9]

Especially, a dynamic state (mobility) of water molecules may be of interest, because it may reflect the degree of interaction with the surrounding polymer phase. The differential scanning calorimetry (DSC)[4–6] appears as one of useful techniques for evaluating such a dynamic state of water. According to Nakamura et al.,[4] the absorbed water in solid polymers may be classified to following three types: "free water" showing the same freezing behavior as pure bulk water, "freezable bound water" being frozen at lower temperature than free water, "nonfreezing bound water" with no exothermic peak due to crystallization in the DSC cooling curve. In addition, the content of freezable bound water calculated by the exothermic peak in a DSC curve was revealed to clearly correlate with the degree of hydrogen bonding with polymers.[4]

Thus investigating the DSC behavior of absorbed water under cooling process may provide valuable information of microstructure of solid polymer phase surrounding the water molecules. Kawagoe et al.[10] has characterized the matrix/fiber interfacial region in a polyamide 6 (PA6)/carbon fiber model composite by comparing the DSC behavior of absorbed water with that in neat PA6 under cooling process. They revealed a clear exothermic peak due to crystallization of water, and thus suggested that in the model composite a part of water molecules behaves as free water or freezable bound water in some heterogeneous microstructure like voids in the interfacial region, probably induced during a process of containing carbon fibers, while in the neat specimen the water totally exists as nonfreezing bound water showing no exothermic peak of DSC. Their investigation suggests such DSC analyzes of absorbed water to also be effective for characterizing the microstructure of plastically deformed polymers, in which the microstructural heterogeneities like voids are also generated.[11–13]

In this connection, the thermoporosimetry is of great interest. This method has been developed by Ishikiriyama et al.[14,15] to estimate the pore size distributions in the porous materials from the DSC freezing curve of absorbed water. They applied the dynamic and thermodynamic relationships derived

*Correspondence to:* M. Kawagoe (kawagoe@pu-toyama.ac.jp).

from the Laplace and Gibbs-Duhem equations to a DSC freezing curve of liquid water in the pores. They demonstrated for several kinds of silica gel that the estimated results by the thermoporosimetry are in good agreement with the measurements by nitrogen gas adsorption–desorption and mercury porosimetry. By applying their method, it is expected to obtain more detailed information of the microstructure of solid polymers from the DSC curve for water freezing.

In view of the above, we have examined the absorption and freezing behavior of water in the elongated specimen of PA6 in relation to the change of polymer microstructure by plastic deformation. The weight gain measurements and the DSC investigations under cooling were conducted for the PA6 specimens, which were preliminarily elongated to several levels, and then immersed in distilled water. As a quantitative evaluation of polymer microstructure, the pore size distribution was estimated from the DSC curve for freezing process of absorbed water by the above thermoporosimetry. In addition, the dynamic viscoelastic behavior also has been examined for the elongated PA6. Based on these analyzes the microstructural changes of PA6 by elongation were discussed from a view point of the existing state of absorbed water.

## EXPERIMENTAL

### Material and sample preparation

The material used in this study was a commercially available pellet of PA6 (Ube Industries, Japan; Ube Nylon 6 S1013NW8).

The pellets were preliminarily dried at 80°C at a lowered pressure of about 9.3 kPa for 3 h in a vacuum chamber (Shibata Scientific Technology, Japan; VOR-300). The pellets of about 8.0 g filled in a rectangular mold of stainless steel were preheated at 250°C for 4 min, and compressed at about 15 MPa for 3 min by means of a hot press equipment (Imoto Machinery, Japan; IMC-180), and then cooled slowly to room temperature. The PA6 sheet removed from the mold was cut into rectangles. The small notches were introduced into the both sides of central area of each rectangle to give large elongation. Finally the PA6 specimens with dimensions of 95 × 6 × 0.5 mm were finished by polishing the cut surfaces with abrasive papers of No. 400 and 1000.

### Preparation of elongated samples

The specimens were loaded under tension until fracture in air (RH 50% ± 10%) at room temperature (20°C ± 5°C) for gauge length of 15 mm by using an Instron-type testing machine (Shimadzu, Japan; AG-50kNE). The tests were carried out in a displacement-controlled mode at a fixed crosshead speed of 0.5 mm/min. In this study, for ease, the elongational behavior was described by the nominal stress and the nominal strain calculated from the changes of load and gauge length of specimen, respectively.

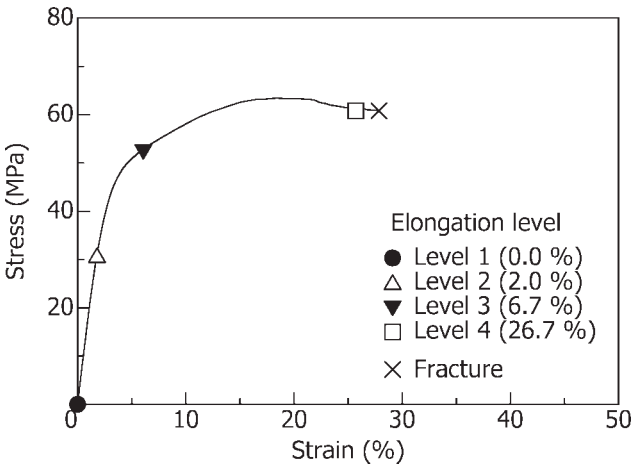


**Figure 1** Typical stress–strain curve of the PA6 specimen.

The specimen showed the tensile strength of about 60 MPa and ductility of about 30.0%, as shown in a typical stress–strain curve in Figure 1. On the basis of this figure, the specimens were prepared by elongation to following different levels: the elongation level 1 at the strain of 0.0% (nonelongation); the level 2 at the strain of about 2.0% (elastic deformation); the level 3 at the strain of about 6.7% (just after beginning of plastic deformation); the level 4 at the strain of about 26.7% (just before fracture). The elongated area of each specimen was cut into small rectangles for each experiment described later.

### Measurement of water content

After preliminary drying in the aforementioned vacuum chamber at room temperature at a lowered pressure of about 9.3 kPa for 18 h, the rectangular small specimens (15 × 4 × 0.3–0.5 mm) were immersed in a beaker of distilled water at 20°C set in a temperature-controlled oven (Tokyo Rika, Japan; KCL-1000). Subsequently the weight was periodically measured by an electronic balance (Mettler-Toledo, Switzerland; AE-240) with a resolution of 0.01 mg until the saturation. The water content was calculated from the weight gain against the initial weight of dried specimen.

### Dynamic viscoelastic test

The dynamic viscoelastic properties were evaluated for the nonelogated (level 1) and largely elongated (level 4) specimens by using a dynamic mechanical

analyzer (SII NanoTechnology, Japan; DMS6100). The specimens with gauge length of 10 mm were subjected to a sinusoidal tensile oscillation at an amplitude of 10.0 μm and a frequency of 1.0 Hz. The storage modulus, $E'$, and loss tangent, tan δ, were measured as a function of temperature ranging from −70 to 100°C at a scanning rate of 2.0°C/min.

### DSC measurements

The water-soaked specimens were cut into a small circle of about 3.0 mm diameter, and then sealed in an aluminum pan. The thermal behavior of the above specimen was analyzed by means of a heat-flow type DSC (SII Nano Technology, Japan; DSC6100) with a cooling device from room temperature to −70°C at a rate of 2.0°C/min. The alumina ($Al_2O_3$) powder was used as a reference matter.

## RESULTS AND DISCUSSION

### Effects of elongation on water absorption

The typical water absorption behavior by the specimen elongated to each level is shown in Figure 2, where the abscissa is expressed by the square root of immersion time per the unit thickness, $t^{1/2}/l$, for considering the difference in the thickness of each specimen by the elongation.

An increase in the water content, $M_t$, is nearly proportional to the square root of immersion time irrespective of elongation level, whereas both a rate of water absorption indicated by a gradient of each curve and an equilibrium water content given by a saturated value are increased with increasing the elongation level, particularly for the level 4. Such a water absorption behavior was approximated by the Fick's law, and then the diffusion coefficient, $D$, were calculated by the following equation[1]:

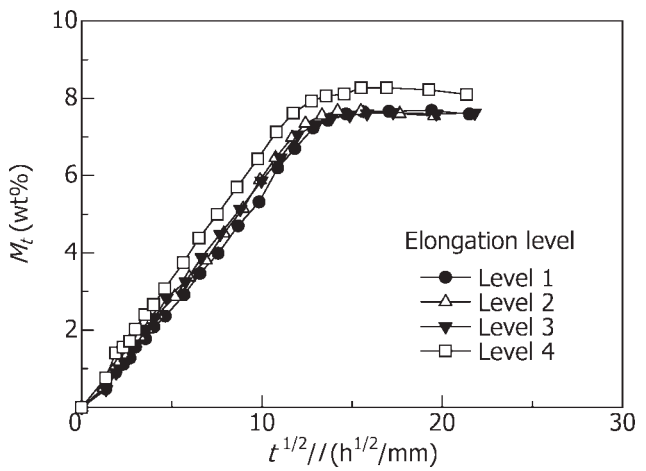


**Figure 2** Typical water absorption behavior by the PA6 specimens.

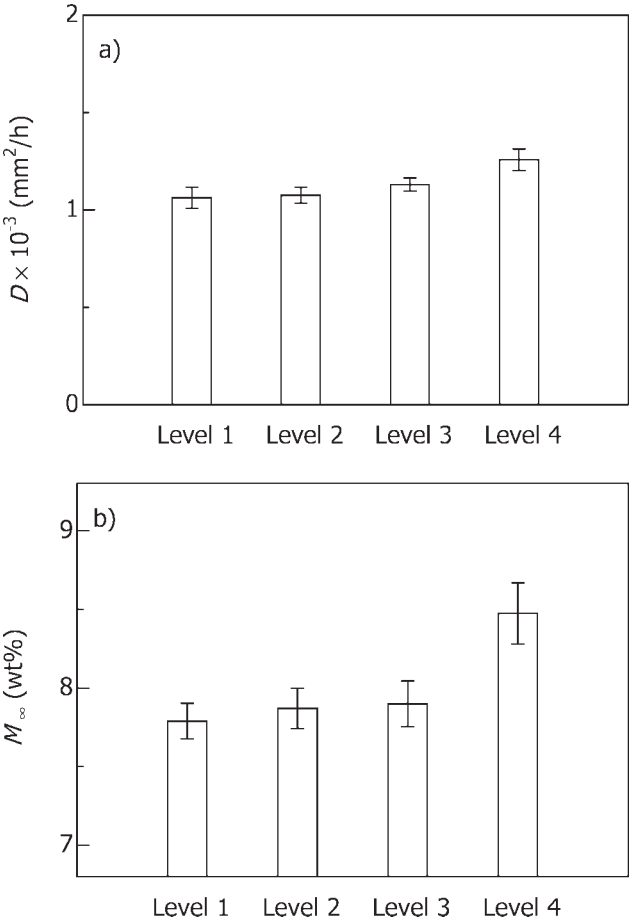


**Figure 3** Changes in water absorption behavior by the elongation: (a) the diffusion coefficient, $D$, and (b) the equilibrium content, $M_\infty$.

$$\frac{M_t}{M_\infty} = 4\left(\frac{D}{\pi}\right)^{1/2}\frac{t^{1/2}}{l}, \quad (1)$$

where $M_\infty$ is the equilibrium water content. The diffusion coefficient and the equilibrium water content for each elongation level are shown in Figure 3(a,b), respectively.

Both the diffusion coefficient and the equilibrium water content are increased with increasing the level of elongation, as shown in Figure 3. Particularly, the diffusion coefficient and the equilibrium water content are greatly enhanced to about $1.3 \times 10^{-3}$ mm$^2$/h and 8.5 wt %, respectively, for the specimen elongated to level 4, compared with those to level 1 (nonelongation) showing about $1.1 \times 10^{-3}$ mm$^2$/h and 7.8 wt %, respectively. Since the water is considered to be absorbed only by an amorphous region, these results suggest an increase in this region by elongation. We have previously evaluated the variation in the degree of crystallinity of PA6 followed by elongation by DSC measurements on the melting enthalpy, and indicated that the degree of crystallinity was decreased from 30.0% to 28.7% by the process

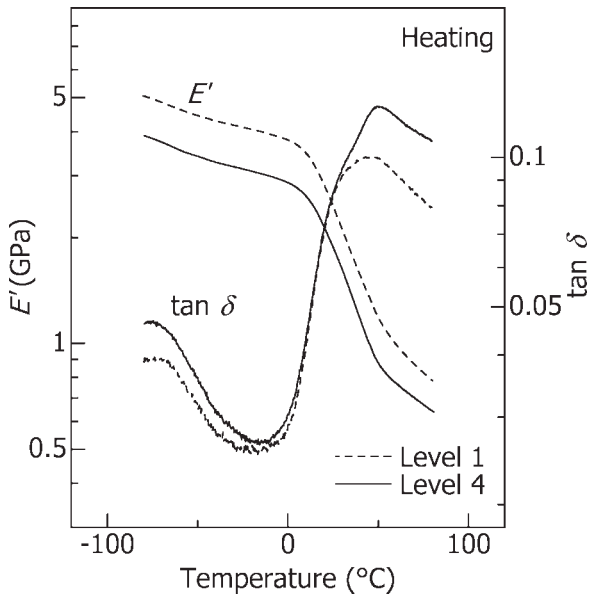


**Figure 4** Effects of the elongation on the dynamic viscoelasticity of dried PA6 specimen.

of elongation from level 1 to 4.[16] These results may indicate that some crystals are collapsed by the large elongation, and as a result the sites possible to absorb water are also increased.

### Effects of elongation on dynamic viscoelasticity

The effects of elongation on the dynamic viscoelasticity of the dried specimen are shown in Figure 4. Compared with the nonelongated specimen (level 1), in the largely elongated specimen (level 4) the tan δ peaks corresponding to the α-relaxation at about 45°C and the β-relaxation at about −70°C are commonly raised,[17] but $E'$ is lowered over the whole temperature range. These variations in the viscoelastic properties suggest that the large and localized scale segmental motions in amorphous region are promoted by the pre-elongation to higher level. It is further supposed that some PA6-intermolecular hydrogen bondings in the crystals may be broken along with the collapse of crystals by large elongation. Such microstructural changes may promote the water penetration, as discussed above for $D$ and $M_\infty$.

### Freezing behavior of absorbed water

The DSC results of water-soaked specimens are shown in Figure 5, where all the curves are weight-normalized to a sample weight of 5.0 mg. The exothermic peak corresponding to freezing of distilled water was detected at about −16.5°C by a preliminary measurement under the same condition. Such a depression of freezing temperature of distilled water has been reported in other study.[4] The mobility of absorbed water in the PA6 specimens was evaluated on the basis of this result.

The DSC cooling curve of the nonelongated specimen (level 1) shows no exothermic peak, despite a considerable amount of absorbed water of about 7.8 wt %. This result supposes that the water molecules in this specimen are strongly restricted to the hydrophilic site of amide group of PA6 through the hydrogen bonding, and are in a state of nonfreezing bound water which cannot be frozen at all.[17] The results for the elongation levels 2 and 3 also show no peak. The large exothermic peak, however, is clearly detected at about −34.5°C on the curve for the elongation level 4, being in a marked contrast to others. In addition, several smaller peaks are also detected at higher temperatures from about −33.0 to −23.0°C. These peak temperatures are also lower than that of distilled water mentioned above. These results thus indicate the presence of freezable bound water, reflecting different degrees of interaction with PA6. Considering the above discussion on the water absorption and the viscoelastic behavior of elongated specimen, it is suggested that some microstructural defects like voids exist in the largely elongated specimen (level 4), being formed by the collapse of crystals.[11–13] The water molecules may be accumulated in such defects under much weaker interaction with the surrounding polymer chains.

Assuming small pores as structural defects, the pore size distribution is analyzed by applying the method of thermoporosimetry developed by Ishikiriyama et al.[14,15] to the DSC curve for the largely elongated specimen (level 4). In their method the pore size distribution in a porous material is estimated by applying the Laplace and Gibbs-Duhem equations to freezing behavior of liquid water in the pore, which is evaluated by DSC under cooling. The

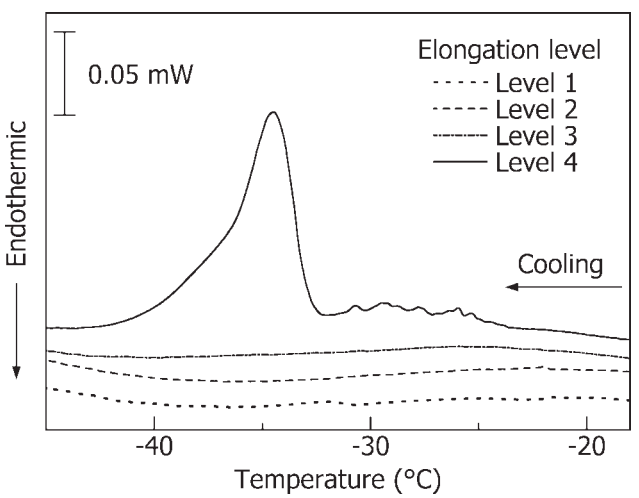


**Figure 5** DSC cooling curves of the elongated PA6 specimens soaked in water at 20.0°C (cooling rate at 2.0°C/min).

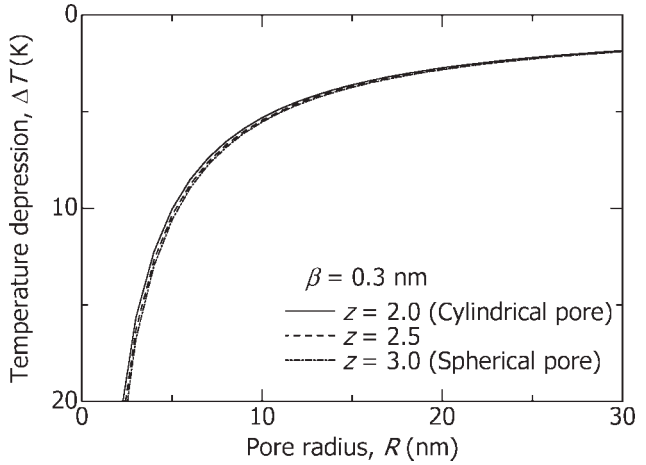


**Figure 6** The freezing temperature depression of water in the pores, $\Delta T$, as a function of the pore radius, $R$, and the pore shape factor, $z$, being calculated using the parameter at $\beta = 0.3$ nm.

pore size estimation by their method has been confirmed by comparison with the experimental results for several kinds of silica gel by nitrogen gas adsorption-desorption and mercury porosimetry. The theoretical estimation was demonstrated to agree well with the experimental results. Thus their method seems to be sufficiently effective to estimate the pore size distribution, and consequently further verifications by the actual measurements using a transmission electron microscopy and the above methods were not conducted in this study.

According to their method of thermoporosimetry, the abscissa and the ordinate of DSC cooling curve of freezable water given in Figure 5 are transformed into the pore radius and the change in the pore volume, respectively. The pore radius, $R$, is given by the following equation[14,15]:

$$R = \frac{\alpha}{\Delta T} + \beta, \tag{2}$$

where $\alpha$ is determined as a function of temperature, $T$, for a pore shape factor, $z$, as follows[14,15]:

$$\alpha = 56.36 - 0.9024\,\Delta T \quad \text{at } z = 2.0 \text{ (for cylindrical pore)}, \tag{3}$$

$$\alpha = 57.26 - 0.8164\,\Delta T \quad \text{at } z = 2.5, \tag{4}$$

$$\alpha = 57.80 - 0.7444\,\Delta T \quad \text{at } z = 3.0 \text{ (for spherical pore)}, \tag{5}$$

where $\Delta T$ is the freezing temperature depression of a freezable pore water, and $\beta$ is a layer thickness of nonfreezable pore water existing on a pore surface. In this study $\beta$ is simply set to 0.3 nm, supposing a layer of one molecular size of water.[18] The freezing temperature depression, $\Delta T$, calculated from eq. (2) is greatly increased with decreasing the pore radius, as shown in Figure 6. The ordinate of DSC curve showing the heat flow, $dq/dt$, is transformed into the variation in the cumulative pore volume, $dV_p/dR$, by the following equation[14,15]:

$$\frac{dV_\mathrm{p}}{dR} = \left|\frac{dq}{dt}\right| \frac{dt}{dR} \frac{1}{m\Delta H_m \rho_\mathrm{fp}} \frac{R^z}{(R-\beta)^z}, \tag{6}$$

where $m$ is the weight of specimen, and $\rho_\mathrm{fp}$ is the density of freezable pore water, which is assumed to be the same as that of bulk water.[14] In addition, $\Delta H_m$ is the heat of phase transition of the freezable pore water, which is also assumed to be the same as bulk water.[14]

The estimation of pore size distribution was conducted in the above way for the DSC curve on the largely elongated specimen (level 4) given in Figure 5. The result is shown in Figure 7, which shows three curves of pore size distribution corresponding to $z = 2.0$, 2.5, and 3.0. The pore radius ranges from about 1.8 to 7.0 nm, showing the highest peaks at about 2.5, 2.6, or 2.7 nm, respectively. The porosity parameters including the total pore volume, $V_p$, the internal surface area, $S_p$, and the average pore radius, $R_\mathrm{ave}$, are calculated from these distributions by the following equations:

$$V_p = \int_0^\infty \left(\frac{dV_\mathrm{p}}{dR}\right) dR, \tag{7}$$

$$S_\mathrm{p} = \int_0^\infty \frac{z}{R}\left(\frac{dV_\mathrm{p}}{dR}\right) dR, \tag{8}$$

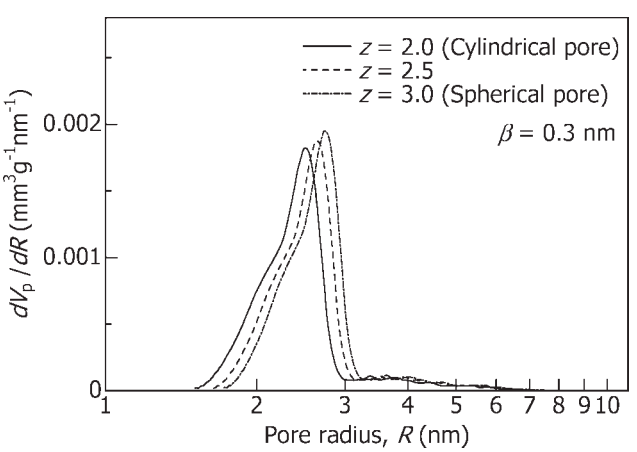


**Figure 7** The pore size distribution in the largely elongated specimen (level 4) on the basis of the thermoporosimetry, being calculated using the parameter at $\beta = 0.3$ nm.

**TABLE I**
**Porosity Parameters for Elongated Specimen to Level 4**

| $Z$ | $V_p$ ($mm^3\ g^{-1}$) | $S_p$ ($m^2\ g^{-1}$) | $R_{ave}$ (nm) |
|---|---|---|---|
| 2.0 | $13.5 \times 10^{-4}$ | 1.1 | 2.5 |
| 2.5 | $14.1 \times 10^{-4}$ | 1.4 | 2.6 |
| 3.0 | $14.8 \times 10^{-4}$ | 1.6 | 2.7 |

$$R_{ave} = \frac{zV_p}{S_p}. \quad (9)$$

The results are shown in Table I. These estimated results indicate that many pores are of about 1.8–10.0 nm in radius, mainly of about 2.5–2.7 nm, for the cylindrical and the spherical pores ($z = 2.0$–$3.0$). In this sence these pores are appropriate to be classified to mesopores. These mesopores are characterized to have $V_p$ of about $13.5 \times 10^{-4}$ $mm^3\ g^{-1}$, $S_p$ of about 1.1 $m^2\ g^{-1}$, and $R_{ave}$ of about 2.5 nm in case of cylindrical pore ($z = 2.0$). Such mesopores may be formed by the collapse of crystals during the large elongation, as discussed earlier.

## CONCLUSION

We have investigated the water absorption behavior by the polyamide 6 specimens, which were preliminarily elongated to various levels, and then immersed in distilled water at 20°C. Both the diffusion coefficient and the equilibrium content of water were increased by large plastic elongation. As for the dynamic viscoelastic behavior, the storage modulus was lowered, and the loss tangents for α- and β-relaxations were commonly raised by large elongation. The DSC measurements were conducted under cooling for the water-soaked specimen. Several exothermic peaks indicating the presence of freezable bound water were clearly observed in the largely elongated specimen. These results suggest that the large elongation causes the collapse of crystals to make some structural defects like voids, in which the water molecules are accumulated under much weaker interaction with the surrounding polymer phase. Such structural defects (voids) were supposed to be pores, and analyzed on their size on the basis of thermoporosimetry. Assuming all the pores to be cylindrical, they were characterized to have the average radius of about 2.5 nm, being appropriately classified to mesopore.

The authors thank Associate Professor K. Sanada, Toyama Prefectural University, for valuable discussions. They also thank M. Itou, S. Tanihara, K. Urakami, and Y. Nakamura for their help in the experiments.

## References

1. Comyn, J., Ed. Polymer Permeability, Elsevier Applied Science: New York, 1985.
2. Kusanagi, H.; Yukawa, S. Polymer 1994, 35, 5637.
3. Lim, L. T.; Britt, I. J.; Tung, M. A. J Appl Polym Sci 1999, 71, 197.
4. Nakamura, K.; Hatakeyama, T.; Hatakeyama, H. Polymer 1983, 24, 871.
5. Higuchi, A.; Iijima, T. Polymer 1985, 26, 1207.
6. Ping, Z. H.; Nguyen, Q. T.; Chen, S. M.; Zhou, J. Q.; Ding, Y. D. Polymer 2001, 42, 8461.
7. Luo, S.; Leisen, J.; Wong, C. P. J Appl Polym Sci 2002, 85, 1.
8. Shinyashiki, N.; Matsumura, Y.; Miura, N.; Yagihara, S.; Mashimo, S. J Phys Chem 1994, 98, 13612.
9. Boinard, P.; Boinard, E.; Pethrick, R. A.; Banks, W. M.; Crane, R. L. Sci Eng Comp Mater 1999, 8, 175.
10. Kawagoe, M.; Nabata, M.; Ishisaka, A. J Mater Sci 2006, 41, 6322.
11. Friedrich, K. Crazing in Polymers, Kausch, H. H., Ed. Springer-Verlag: Berlin, 1983; pp 225.
12. Butler, M. F.; Donald, A. M.; Ryan, A. J. Polymer 1997, 38, 5521.
13. Butler, M. F.; Donald, A. M.; Ryan, A. J. Polymer 1998, 39, 39.
14. Ishikiriyama, K.; Todoki, M.; Motomura, K. J Colloid Interface Sci 1995, 171, 92.
15. Ishikiriyama, K.; Todoki, M. J Colloid Interface Sci 1995, 171, 103.
16. Sakai, E.; Kawagoe, M. Koubunshi Ronbunshu 2008, 65, 355. (In Japanese)
17. Fukumoto, O., Ed. Polyamide Resin Handbook, Nikkan Kougyo Shinbunsha: Tokyo, 1988. (In Japanese).
18. Kaewnopparat, S.; Sansernluk, K.; Faroongsarng, D. AAPS PharmSciTech 2008, 9, 701.